Electronic Supplementary Material (ESI) for Green Chemistry.

Supporting Information for

Cost and Energy Efficient Cyclic Separation of 5-hydroxymethyl Furfural from an Aqueous Solution

Yung Wei Hsiao, Aikaterini Anastasopoulou, Marianthi Ierapetritou, and Dionisios G. Vlachos*
Department of Chemical and Biomolecular Engineering, University of Delaware, 150 Academy Street, Newark, Delaware 19716, United States
RAPID Manufacturing Institute, Delaware Energy Institute (DEI), University of Delaware, 221 Academy Street, Newark, Delaware 19716, United States

Adsorbent Characterization

Morphological characteristics of adsorbents used for HMF adsorption in the literature.

Table S1: Textual properties of adsorbent existing in the literature.

Adsorbent Type	Manufacturer	Particle Size	Surface area (m^2/g)	Pore Volume (cm^3/g)	Oxygen Content (Various)
BP2000[1–3]	Cabot Norit	20-100nm	1374	2	0.0185 (Atomic molar ratio) (Minimal carboxylate groups) 9.5% oxygen content
Polymer Based Spherical Activated Carbon (PBSAC-100043)[This work]	Blucher GmbH, Erkrath, Germany	0.1-0.315mm	1085 (reported 1796)	0.899	4.6% oxygen content
Polymer Based Spherical Activated Carbon (PBSAC-200) (100050)[4]	Blucher GmbH, Erkrath, Germany	0.2-1mm	1889	0.8875	<5wt% oxygen content <1.5wt% C=O <3wt% C-O
Hollow-structured porous aromatic polymers (H-PAP)[5]	In-lab synthesis	Length 464 nm Thickness: 34nm	890	0.72	Water contact angle of 110.9
Nanoporous Hyper Cross-Linked Polymers (HCP)[6]	In-lab synthesis using Friedel-Crafts Alkylation Method	<0.2mm	2398	3.73	Water vapor physisorption of <1% at p/p0 = 0.9
Metal Organic Framework (NU-1000)[7]	In-lab synthesis	Rod shape W ~ 0.5-1um, L ~ 5um	2320	1.4 (only ~0.495 utilized)	-
Zeolitic Imidazolate Frameworks (ZIF-8)[8]	In-lab synthesis	3.2-5.2um	1339	0.598	Carboxylate-based No reported oxygen ratio
H-BEA (Si:Al = 18) Zeolite[9]	Zeolyst International (thermal treatment) (CP814N)	powder (nm)	600-700	0.177	SiO_2/Al_2O_3 = 18

Morphological characteristics of PBSAC were studied in-house using nitrogen physisorption and XPS.

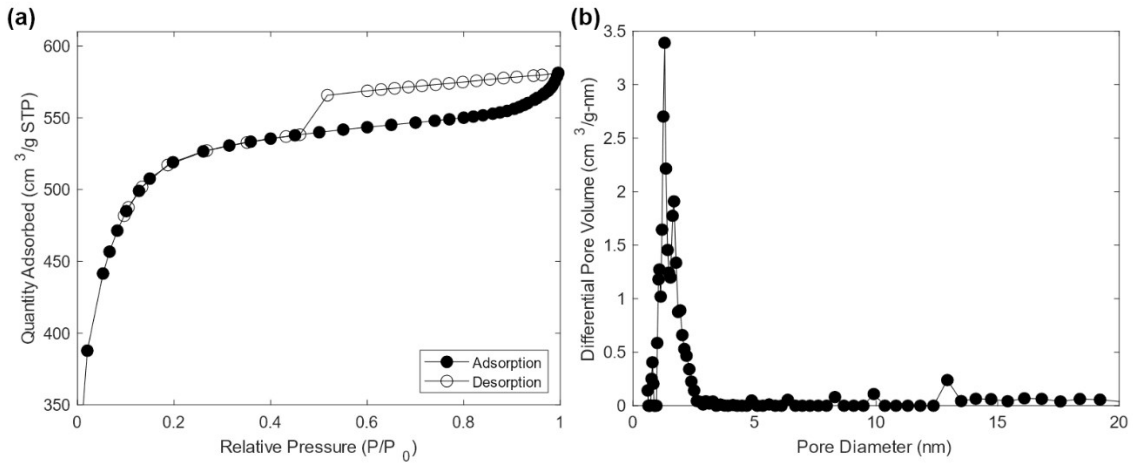

Figure S1: (a) Nitrogen physisorption adsorption-desorption isotherm and (b) Barrett-Joyner-Halenda (BJH) pore size distribution.

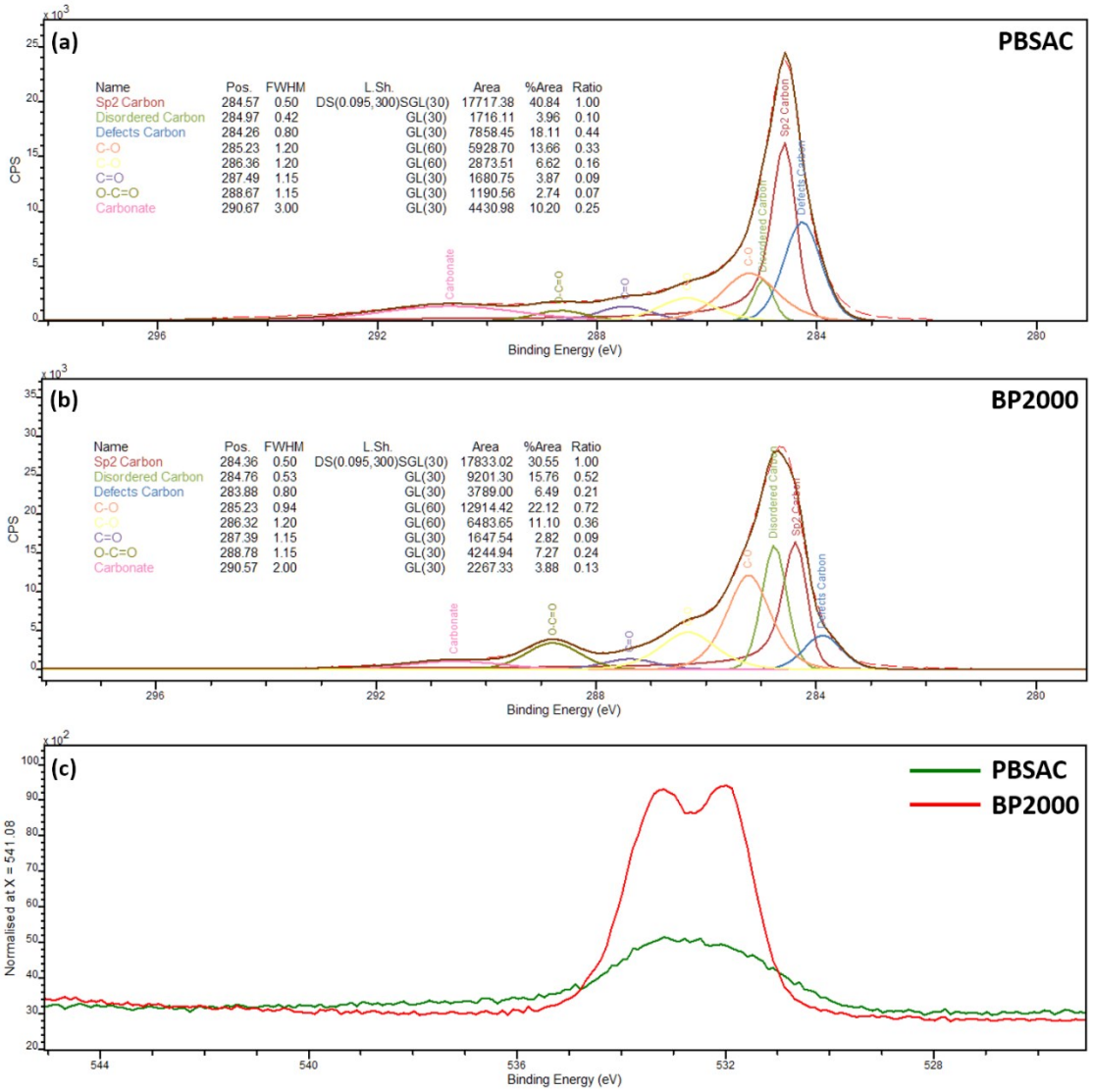

Figure S2: C1 scans of (a) PBSAC and (b) BP2000, and (c) O1 scans of PBSAC and BP2000 overlaid.

Packing Effectiveness

The asymmetry factor is calculated as the ratio of the rear half-width (b) over the front half-width (a) of the elution peak. These half widths are determined at 10% of the peak height. A MATLAB script was used to auto-detect the locations and heights of the peak, and subsequently calculate the two widths. The asymmetry factor characterizes the tailing profile, where a ratio >>1 correlates to channeling. An acceptable asymmetry factor should be between 0.8 and 1.5-1.8.[10] Columns in this study had asymmetric factors between 1.4 and 1.6, and if outside this range, they were discarded.

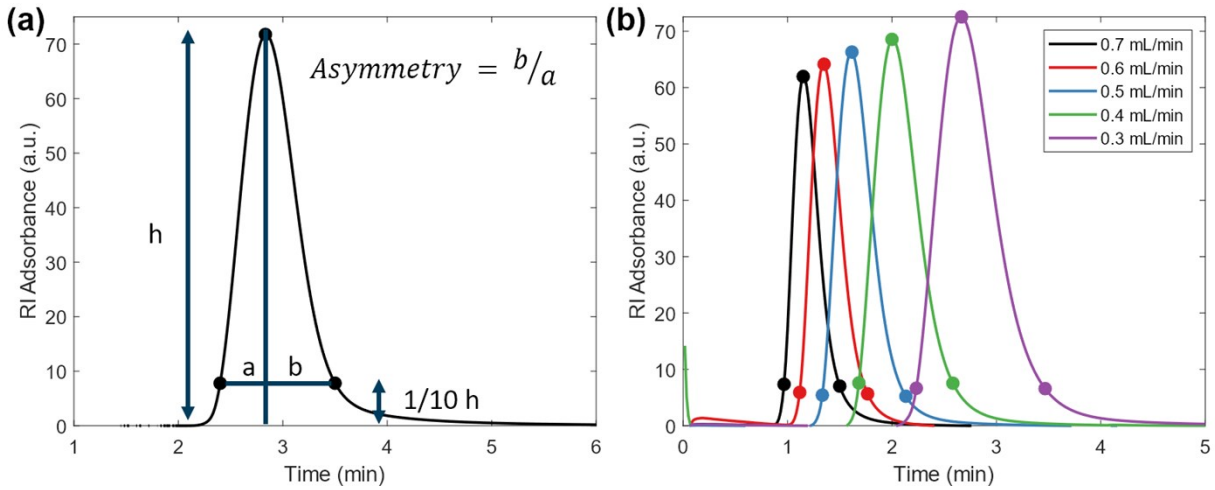

Figure S3: Asymmetry factor of a fixed-bed. (a) Calculation of asymmetry factor as the ratio of the back to the front peak at 1/10 of the tracer peak height. A ratio <1 is known as fronting, and a ratio > 1 is correlated to channeling in the column. Different flowrates were tested to validate the calculation of the asymmetry factor.

Experimental Assessment of the Continuous Setup

As shown in Scheme 1, the use of a 4-way manifold to merge the more concentrated solute solution with the preheated solvent stream prior to entering the column minimizes potential temperature degradation of the solute, notably fructose and FA, in the slightly acidified water stream at higher temperatures. The inlet concentration and temperature were tested using a control column packed with inert glass beads to simulate a similar residence time. Each channel of the manifold was connected to the solute stream, the water stream, a thermocouple, and the inlet of the column. A Tee was connected to the end of the column, a thermocouple, and the exit stream. The temperatures at the inlet and outlet of the column were monitored using the same thermometer. The total flowrate was held constant at 1.1 mL/min. The solute stream was fed in at room temperature at a lower flowrate to be brought to experiment temperature by the preheated water stream merging in a larger volume. The temperature difference between the two exits when the oven was set at 130 and 150 °C is shown in Figure S4. A flow ratio of 1:10 is optimal because it has a minimal 0.1 °C temperature difference between the two exits and causes the smallest oscillation in pump flowrate and solute concentration due to the pumping force difference. Operation temperatures lower than the ones outlined here are expected to have an even better performance where the temperature gradient is even less.

A100 psi check valve was placed in the solute line before the manifold to introduce an artificially higher pressure for the solute stream. This method facilitates a steadier flowrate for the stream with a smaller flowrate. A small amount of liquid volume – that is filled with water from washing – exists between the check valve and the merging manifold. Since the solute stream has

a low flowrate, this liquid volume can cause a long purge time with an unsteady concentration profile. Fast reactant concentration equilibration is necessary for accurate estimation of a transient system. A manual shut-off valve was placed in front of the 100 psi check valve to introduce a second artificial pressure built up to quickly purge and equilibrate this connection line when the valve was opened. As shown in Figure S5, minimizing the liquid volume for this connection line to 0.005mL and having a 250 psi pressure buildup at the shut-off valve can quickly establish the inlet concentration to C_0 in < 5min without overshooting C_0. These preliminary experiments settle the 1:10 flow ratio and 250 psi pressure buildup for all experiments described in this work.

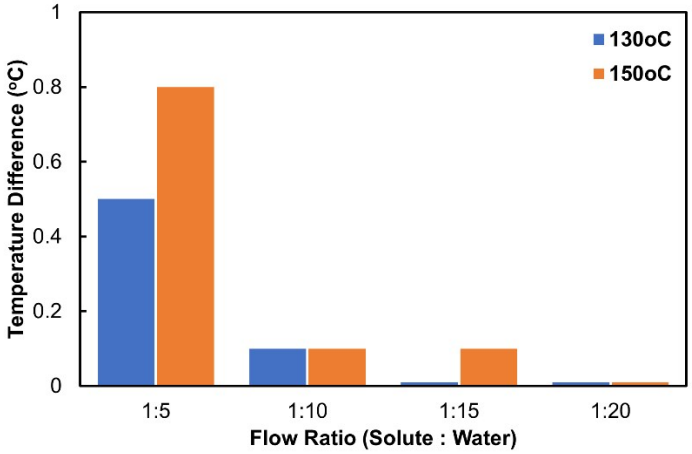

Figure S4: The temperature difference between the inlet and outlet of the adsorption column at different solute to water flow ratios.

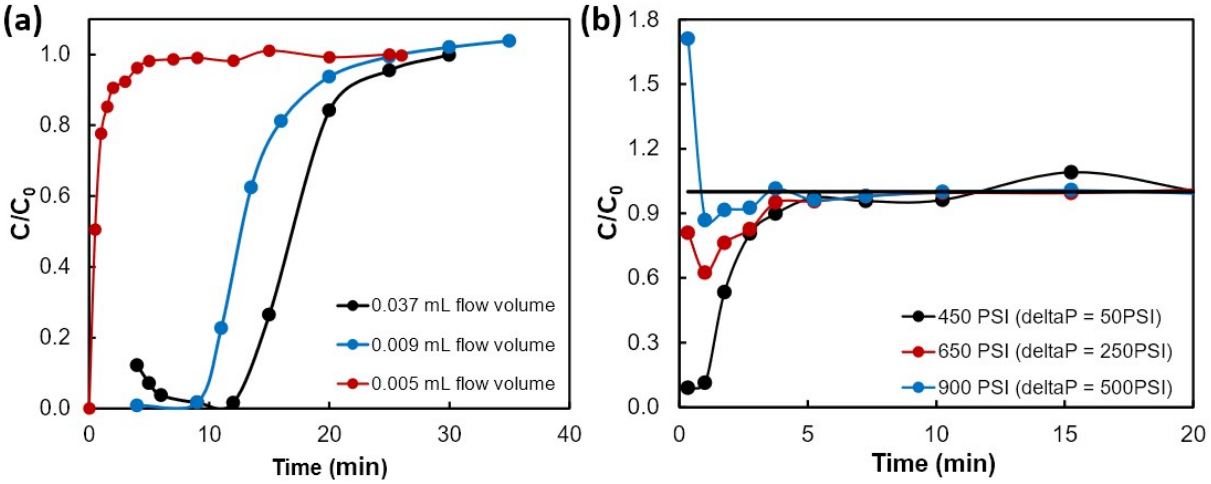

Figure S5: Merge stream concentration vs. time. Effects of (a) the liquid volume between the manual shut-off valve and merging Tee/Cross, and the (b) pressure built up before opening the shut-off valve, in establishing the desired concentration C_0. The flowrates used were 0.1 mL/min for the concentrated solute stream and 1 mL/min for the water stream, leading to a total flowrate of 1.1 mL/min.

Batch Isotherms

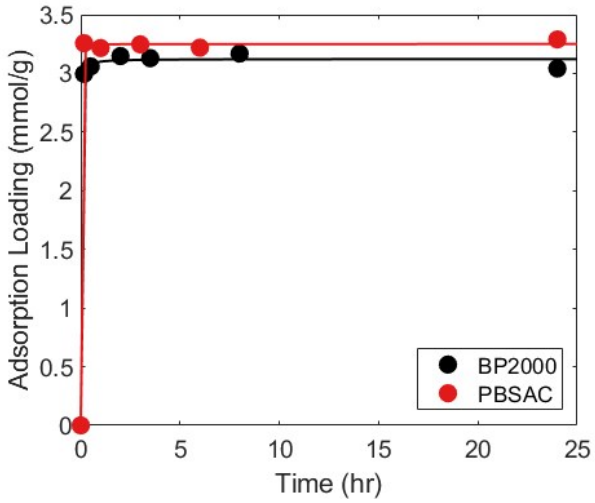

Figure S6: Adsorption loading of HMF over time. The adsorption rates of HMF on PBSAC and BP2000 were determined in batch. Equilibrium is reached within 3 min for both carbons. Therefore, the adsorption rate was assumed not to be rate-limiting.

Batch isotherm results were further fitted using the Freundlich isotherm (Eq. S1) with the result shown in Table S2, where K_F is the Freundlich isotherm equilibrium constant [$(L/g_{carbon})^{1/n}$], and n is an empirical exponent between 0 and 1. This two parameter isotherm is numerically simple to integrate in the Ideal Adsorption Solution Theory (IAST) for predicting multicomponent adsorptions involving four components. Additionally, fructose was fitted using the Langmuir isotherm (Eq. S2) due to good agreement with the model equation, where K_L is the Langmuir isotherm equilibrium constant [(L/g_{carbon})], and b_L is a constant [(M^{-1})]. It is likely that the weak adsorption affinity of fructose on the carbon surface led to weak, single-layered adsorption. The remaining three components show a weak resemblance to the Langmuir isotherm.

$$q_{eq} = K_F C^n \qquad (S1)$$

$$q_{eq} = \frac{K_L C}{1 + b_L C} \qquad (S2)$$

Table S2: Fitted adsorption parameters for four adsorbate species on PBSAC using the Freundlich and Redlich-Peterson models at various temperatures.

Component	Model	Temp. (K)	K (L/g or $(L/g_{carbon})^{1/n}$)	b $(L/mol)^n$	n	R^2
Fructose	Freundlich	298	2.19E-03	-	0.37	0.9279
		338	1.52E-03		0.37	0.8727
		363	1.22E-03		0.37	0.8873
	Redlich-Peterson	298	8.83E-02	82.8	0.95	0.9988
		338	4.52E-02	55.3	0.95	0.9312
		363	3.60E-02	54.7	0.95	0.9586
	Langmuir	298	8.22E-02	1.0	-	0.9979
		338	5.67E-02	0.7		0.9330
		363	5.58E-02	0.6		0.9630
HMF	Freundlich	298	1.10E-02	-	0.32	0.7711
		338	1.05E-02		0.32	0.9319
		363	8.49E-03		0.32	0.9910
		393	6.85E-03		0.32	0.9760
	Redlich-Peterson	298	1.00E+02	1.09E+04	0.77	0.9577
		338	5.88E+01	7.95E+03	0.77	0.9932
		363	6.96E+00	1.13E+03	0.77	0.9974
		393	9.34E-01	1.63E+02	0.77	0.9858
	Redlich-Peterson (Used for Comp Ads Prediction only)	298	1.00E+01	1166	0.77	0.8418
		338	8.65E+00	1130	0.77	0.9546
		363	6.80E+00	1103	0.77	0.9974
FA	Freundlich	298	3.17E-03	-	0.37	0.9911
		338	2.55E-03		0.37	0.9851
		363	2.06E-03		0.37	0.9646
	Redlich-Peterson	298	1.60E-01	53.36	0.78	0.9498
		338	7.85E-02	35.00	0.78	0.9484
		363	4.74E-02	24.95	0.78	0.9404
LA	Freundlich	298	5.55E-03	-	0.24	0.9966
		338	4.89E-03		0.24	0.9962
		363	4.09E-03		0.24	0.9880
	Redlich-Peterson	298	8.91E+00	1.55E+03	0.78	0.9239
		338	4.63E+00	9.58E+02	0.78	0.9934
		363	1.47E+00	3.65E+02	0.78	0.9961

Table S3: Adsorption separation factor of PBSAC as a function of surface adsorption loading and temperature.

Temp. (°C)	Total Adsorption	Adsorption Selectivity

	Loading (mmol/g)	Fructose	HMF	FA	LA
25	0.70	0.11	0.82	0.24	0.34
	1.09	0.09	1.08	0.17	0.34
	1.82	0.04	1.60	0.10	0.33
	3.18	0.01	3.76	0.05	0.17
	3.70	0.01	5.40	0.04	0.12
	4.10	0.01	5.44	0.05	0.11
55	0.66	0.09	0.89	0.21	0.37
	1.00	0.07	1.22	0.15	0.34
	1.67	0.04	1.88	0.09	0.29
	2.84	0.01	3.75	0.05	0.17
	3.33	0.02	4.72	0.05	0.12
	3.99	0.02	3.59	0.09	0.13
90	0.65	0.12	0.87	0.18	0.37
	1.00	0.12	1.14	0.11	0.36
	1.62	0.09	1.68	0.07	0.29
	2.72	0.04	2.64	0.08	0.20
	3.10	0.02	3.80	0.07	0.15
	3.72	0.03	3.11	0.10	0.14

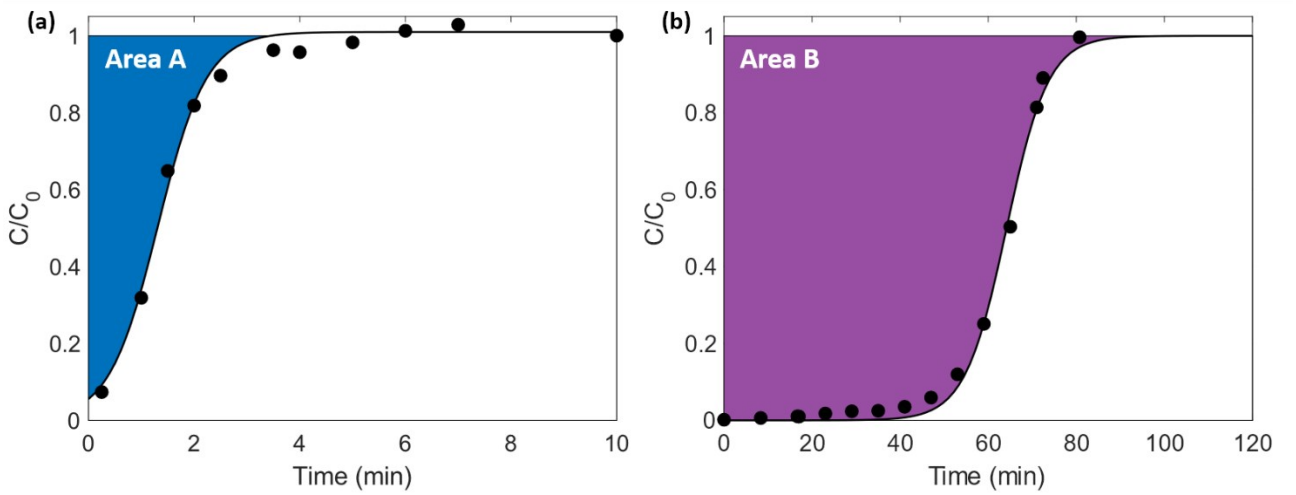

Figure S7: Baseline correction. Actual adsorption loading is calculated as Area B – Area A.

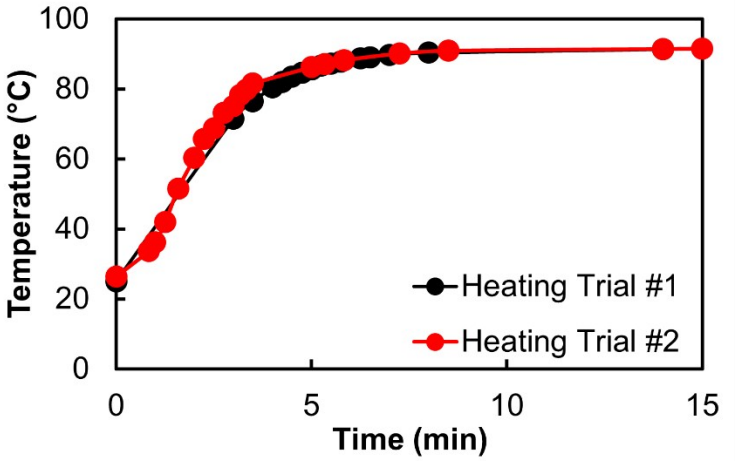

Figure S8: Continuous heating of IPA at a flowrate of 0.55 mL/min from 25 °C to 90 °C inside the GC oven during a desorption experiment for two repeats. It takes 8 min for IPA to reach the set temperature.

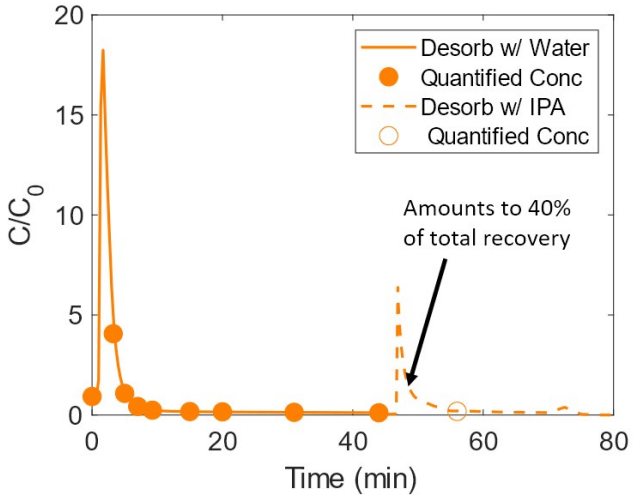

Figure S9: Use of IPA to fully recover all the adsorbed HMF following water desorption.

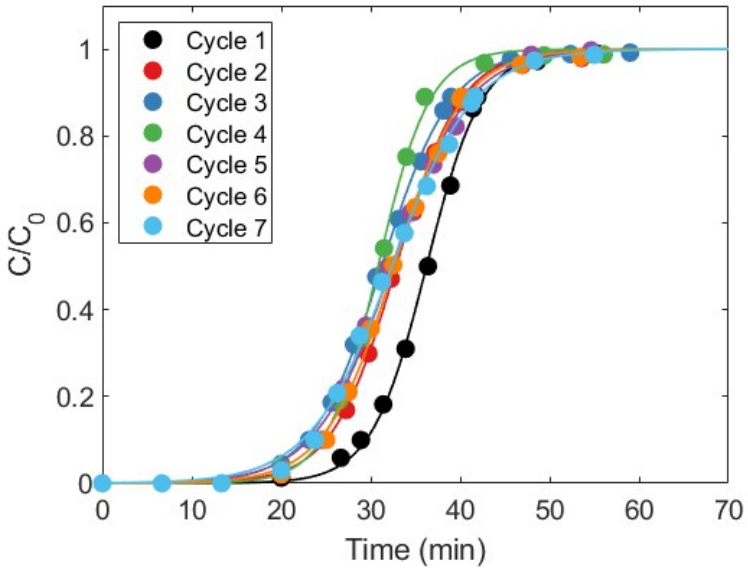

Figure S10: Seven adsorption breakthrough curves of HMF in the same PEEK column following complete HMF desorption. Recovery conditions are as follows: Cycle 1, 2, and 3: IPA at 25 °C; Cycle 4 and 5: IPA at 90 °C; Cycle 6: Water at 90 °C; and Cycle 7: Water at 25 °C. When water was used as the desorbing solvent, full recovery could not be achieved within 45 min; the column was subsequently flushed with IPA for an additional ≥20 min to ensure full HMF recovery for the next cycle, as shown in Figure S9.

Model Predictions

Table S4: Model parameters of fructose, FA, LA and HMF adsorption on PBSAC in water solvent at 25 °C and Q=1.1 mL/min.

Component	C_o [mol/m^3]	q_o [mol/kg]	D_{ax} [m^2/s]	D_f [m^2/s]	Re	Pe	Curve fitting MSE
Fructose	6.89	0.28	3.7E-04	6.90E-10	0.8967	1.14	2.97E-03
FA	26.10	1.04	6.4E-04	1.40E-09	0.8967	0.66	1.77E-03
LA	10.78	2.04	2.9E-04	1.20E-09	0.8967	1.45	1.94E-02
HMF	9.93	3.28	2.8E-04	1.20E-09	0.8967	1.50	2.26E-02

Table S5: Model parameters of HMF adsorption on PBSAC in water solvent at 25 °C and different flow rates.

Flow rate [mL/min)	C_o [mol/m^3]	q_o [mol/kg]	D_{ax} [m^2/s]	D_f [m^2/s]	Re	Pe	Curve fitting MSE
0.55	10.75	3.33	1.80E-04	1.20E-09	0.4076	1.06	2.53E-02
1.1	9.93	3.28	2.50E-04	1.20E-09	0.8967	1.68	9.18E-03
2.2	10.85	4.34	5.20E-04	1.20E-09	1.7935	1.62	5.46E-03

Table S6: Model parameters of HMF desorption on PBSAC in water solvent at Q=0.55 ml/min and different temperatures.

Temp. [°C]	C_o [mol/m^3]	q_o [mol/kg]	D_{ax} [m^2/s]	D_f [m^2/s]	Pe	Curve fitting MSE
25	9.93	3.28	1.44E-04	1.20E-09	1.46	1.27E-03
55	9.93	2.52	5.50E-03	1.20E-09	0.04	3.32E-03
90	9.93	1.97	8.50E-03	1.20E-09	0.02	5.13E-06

Table S7: Model parameters of HMF desorption on PBSAC in IPA solvent at Q=0.55 ml/min and different temperatures.

Temp. [°C]	C_o [mol/m^3]	q_o [mol/kg]	D_{ax} [m^2/s]	D_f [m^2/s]	Pe	Curve fitting MSE
25	9.93	3.28	1.40E-03	1.20E-09	0.15	5.19E-03
55	9.93	2.52	5.00E-03	1.20E-09	0.04	1.78E-04
90	9.93	1.97	5.50E-03	1.20E-09	0.04	7.78E-04

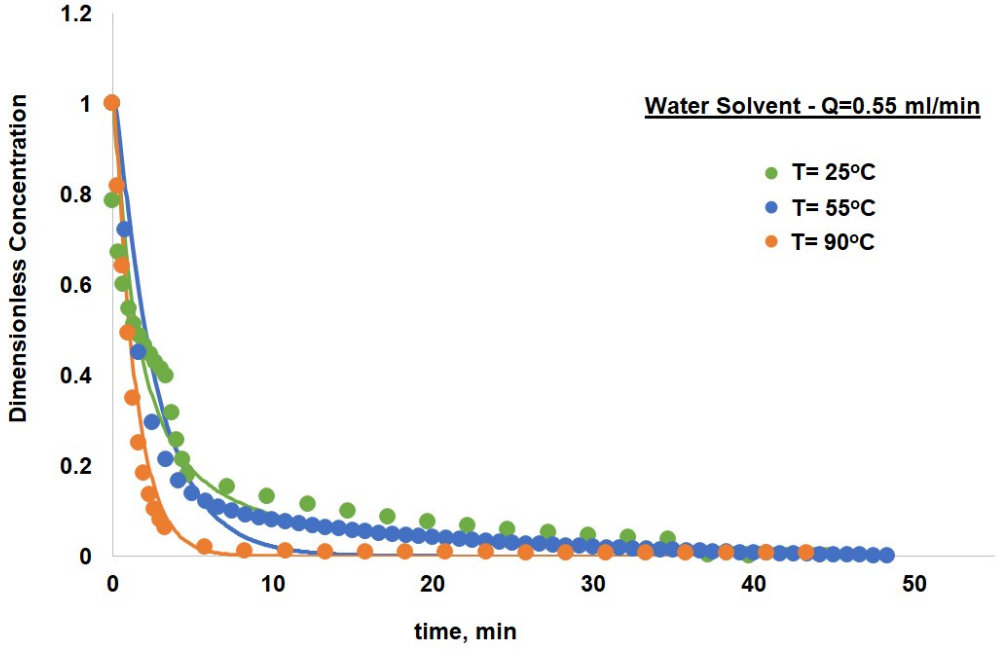

Figure S11: Desorption of HMF in water at a) 25, b) 55, and c) 90°C. Dots are experimental data, and lines are model predictions.

Transport Parameters and Péclet Number Correlations

The dimensionless parameters and their correlations used for comparison with this work are shown in Eq. S3 – S5. The Reynolds (Re) number that predicts fluid flow pattern is the ratio of inertial to viscous forces. The Schmidt number (Sc) that describes the ratio of momentum vs. mass diffusivity was calculated using the molecular diffusion coefficient of the component. Sc was used to estimate the Sherwood number and the external mass transfer coefficient. The Péclet ($P\acute{e}$) correlations[11–13] used for comparison are shown in Eq. S6 – S8. The Galileo number (Ga) is the dimensionless group representing the ratio of gravitational and viscous forces. A liquid holdup volume ($v_{h,t}$) correlation that has been used for the downflow operation of a fixed bed of activated carbon adsorbent was employed to calculate the $P\acute{e}$ value.

$$Re = \frac{\rho d_p v}{\mu} \quad (S3)$$

$$Sc = \frac{\mu}{\rho D_f} \quad (S4)$$

$$Sh = 1.11 * Re^{0.448} Sc^{0.333},\ Sh = \frac{k_f * d_p}{D_f} \quad (S5)$$

$$Ga = \frac{g d_p^3 \rho^2}{\mu^2} \quad (S6)$$

$$v_{h,t} = 3.86 Re^{0.545} Ga^{-0.42} \left(\frac{d_p a_u}{\varepsilon}\right)^{0.65} \quad (S7)$$

$$Pe = \left(\frac{Re}{v_{h,t}}\right)^{0.7} * Ga^{-0.32} \quad (S8)$$

Adsorption at Realistic Concentrations

The adsorption performance of PBSAC at more practical HMF concentrations (e.g., 10 wt%) was studied in both batch and continuous systems.

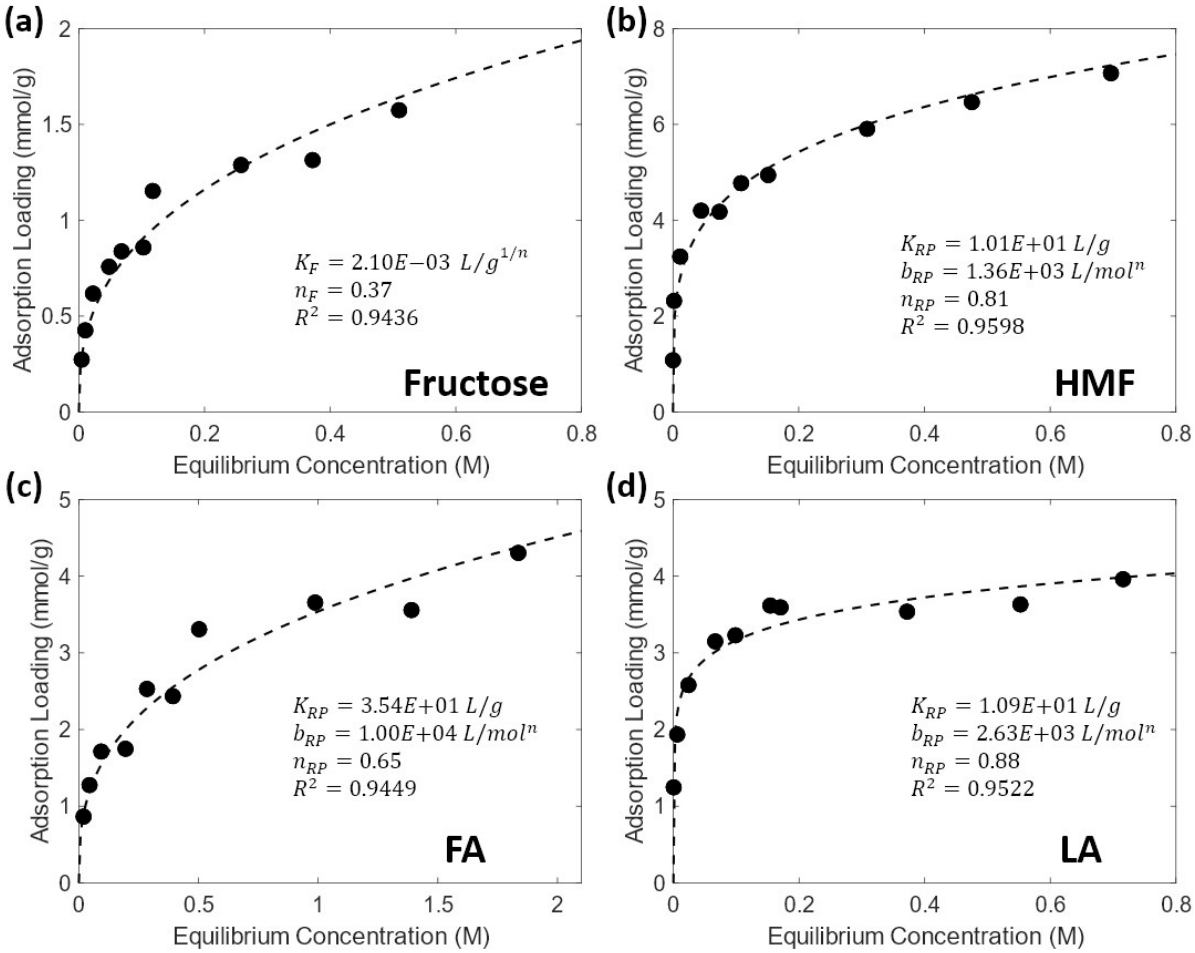

*Figure S12: Experimental adsorption loading (points) and isotherm fits (lines) of **(a)** fructose, **(b)** HMF), **(c)** formic acid (FA), and **(d)** levulinic acid (LA) on PBSAC at 25 °C. Fructose was fitted with the Freundlich isotherm and the rest with the Redlich-Peterson isotherm. Low concentration data from Figure 1 in the manuscript are superimposed with higher concentration data. The isotherm parameters are indicated.*

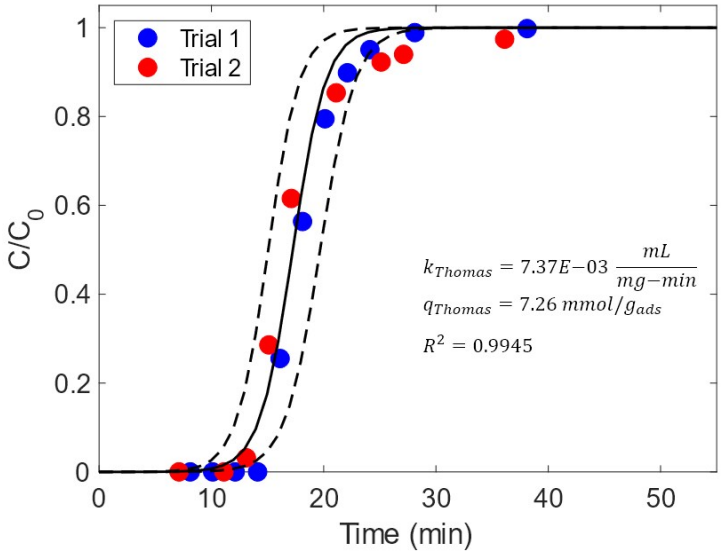

Figure S13: Continuous single component breakthrough curves of HMF at 10 wt% inlet concentration. Points are quantified experimental values, and the solid line is curved fitted using the Thomas model. Dashed lines are 95% confidence intervals from the two trials. Experimental conditions: Temperature = 25 °C, flowrate = 0.2mL/min, and weight of PBSAC = 375 mg. The fitted Thomas parameters are indicated. The adsorption loading of 7.25 mmol/g_{ads} fits well with that from the batch isotherm (7.45 mmol/g_{ads} at 10 wt% equilibrium concentration).

Aspen Simulation

The distillation and vacuum distillation towers were simulated using the RadFrac model in Aspen Plus V11. The properties for both water and HMF were obtained from the Aspen database. The NRTL-RK package was used to simulate the liquid interactions. The minimum number of stages (three trays) was calculated using the McCabe-Thiele method with a reflux ratio of 0.19. Ten stages were used for the simulation. The HMF/water stream was fed into the column at saturation temperature (103 °C) above stage 7. The column pressure drop was set to 0.1 psi, and the condenser pressure drop was 0.5 psi. The heavy key (HMF) purity of 99% was selected as the design specification. This level of purity was achieved by varying the distillate to feed ratio. The operation pressure of the vacuum distillation tower was set to 10 kPa. A vacuum pump was used to reduce the inlet pressure to 23 kPa, and the bottom plate pressure was ~10 kPa. High-pressure (HP) and medium-pressure (MP) steams, and 20 °C cooling water were used for utilities. The equipment and utility costs were estimated using the built-in Aspen Process Economic Analyzer. The process flow diagram is shown in Figure S14, and the abridged results are summarized in Table S4.

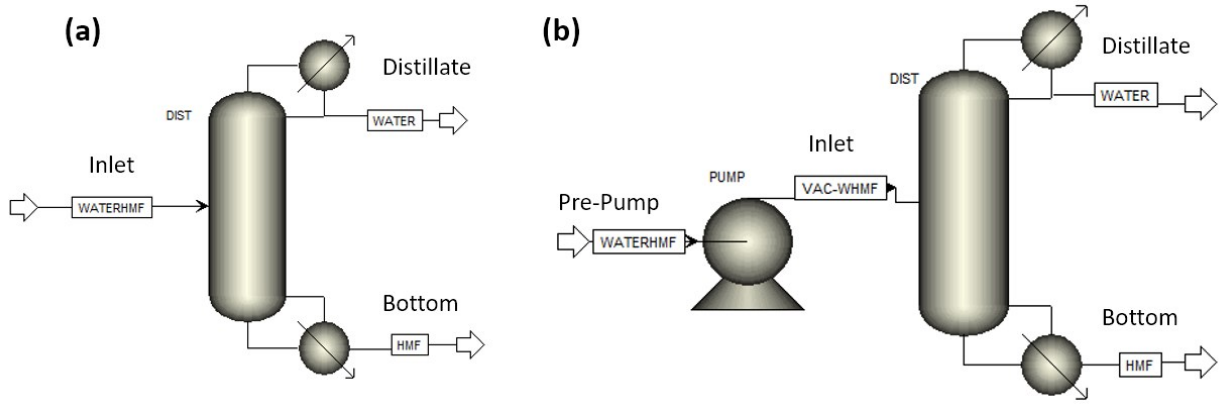

*Figure S14:Process flow diagram of the **(a)** distillation and **(b)** vacuum distillation columns.*

Table S8: Aspen Plus V11 simulation for the purification of HMF.

Single Distillation Column				
Streams		Input	Bottom	Distillate
Temperature (°C)		103.1	200.1	100.0
Pressure (bar)		1.11	1.08	1.01
Phase		Liquid	Liquid	Liquid
Flowrate	HMF (kg/hr)	1250	1250	1.5E-10
	Water (kg/hr)	11250	12.63	11237.37
Mass Fraction	HMF (-)	0.1	0.99	1.3E-14
	Water (-)	0.9	0.01	1
Reflux Ratio		0.19		
Distillate to Feed Ratio		0.90		

Vacuum Distillation Column					
Streams		Pre-Pump	Input	Bottom	Distillate
Temperature (°C)		103.1	103.2	137.5	45.8
Pressure (bar)		1.11	0.22	0.22	0.10
Phase		Liquid	Liquid	Liquid	Liquid
Flowrate	HMF (kg/hr)	1250	1250	1250	4.8E-23
	Water (kg/hr)	11250	11250	12.63	11237.4
Mass Fraction	HMF (-)	0.1	0.1	0.99	4.3E-27
	Water (-)	0.9	0.9	0.01	1
Reflux Ratio		0.19			
Distillate to Feed Ratio		0.90			

Cost	**Single Distillation**	**Vacuum Distillation**
Equipment Cost [$]	$439100	$782600
Total Utilities Cost [$/Year]	$759602	$672628

Adsorption Column Sizing and Cost Estimate

The adsorption capacity, which is temperature-dependent, is a primary design factor. The predicted adsorption capacity of PBSAC at 25 °C at 10 wt% HMF concentration is 7.45 $mmol_{HMF}/g_{ads}$ (based on the Redlich-Peterson isotherm for HMF shown in Figure S12). For adsorption of 30 ton of HMF/day at 25 °C, 40,528 kg of PBSAC is needed (Eq. S9), where f_L is the fraction of the bed loaded at the end of the adsorption phase. Using the experimental breakthrough curve data, a f_L of 0.7825 was calculated as the ratio of the adsorption loading at $\frac{C}{C_0} = 0.01$ and the total loading of a fully saturated column. With an adsorbent density of 0.517 g/cm^3, a bed volume of 78.4 m^3 is necessary. An additional volume (20%) is added for inert material (e.g., ceramic beads) upstream and downstream to ensure a uniform flow at the entry and exit of the bed. The adsorption vessel is sized as a cylindrical pressure vessel of a 2:1 diameter to height ratio. Two columns are used in parallel to ensure continuous operation, where the second column is used when the first bed is being regenerated. For two 304 stainless steel cylinders of 3.91 m in diameter, 7.82 m in height, and 14 mm in wall thickness, the equipment cost is estimated using Eq. S10 to be $226,176, accounting for an 11.5% inflation rate using CEPCI = 594.1 (Aug 2020) and 532.9 (Jan 2010), where C_e is the equipment cost on the US Gulf Coast basis, S is the size parameter (shell mass in kg) of the vessel, and $a, b,$ and n are the cost constants given by Towler & Sinnott.[14] The retail cost of the adsorbent is 42 $/kg, but the bulk prices of adsorbents are in the 0.5 – 1.5 $/kg range. A median value of 1 $/kg price is applied. The total capital cost (column and adsorbent) is ~$307,232. Repurchasing and replacing the adsorbent are not considered, as its frequent replacement may be unnecessary given the good reusability of PBSAC and the lack of long-term usage data. The capacities at elevated temperatures were estimated accordingly, and the same calculations as described above were repeated at each temperature. As shown in Figure S15a, the cost is the lowest at 25°C due to having the highest adsorption capacity.

Alternatively, one could also explore increasing the number of cycles per day and using smaller beds and more regeneration cycles. Since full recovery could be achieved within 25 min at 90 °C using IPA, the processing time is mainly determined from the adsorption cycle. By assuming no time lag between the adsorption and desorption cycles and between the two columns, the adsorber can be scaled down to run more adsorption and desorption cycles in a day. In this case, the processing time is inversely proportional to the number of cycles. Less HMF is processed in each cycle, using less adsorbent in a smaller column size. Using the same approach described above, the costs of the vessel and adsorbent with increasing the number of cycles in a day (smaller vessel sizes) are shown in Figure S15b-d. The Reynolds number calculation using the respective flow velocities indicates a laminar flow regime, and the pressure drop was calculated using the Ergun equation and deemed to be small. Six cycles per day was chosen as a middle ground between cost and the number of cycles in a day.

$$(F_{in} - F_{out})\, time = q_{HMF}\, m_{ads}\, f_L \quad \textit{(S9)}$$

$$C_e = a + bS^n \quad \textit{(S10)}$$

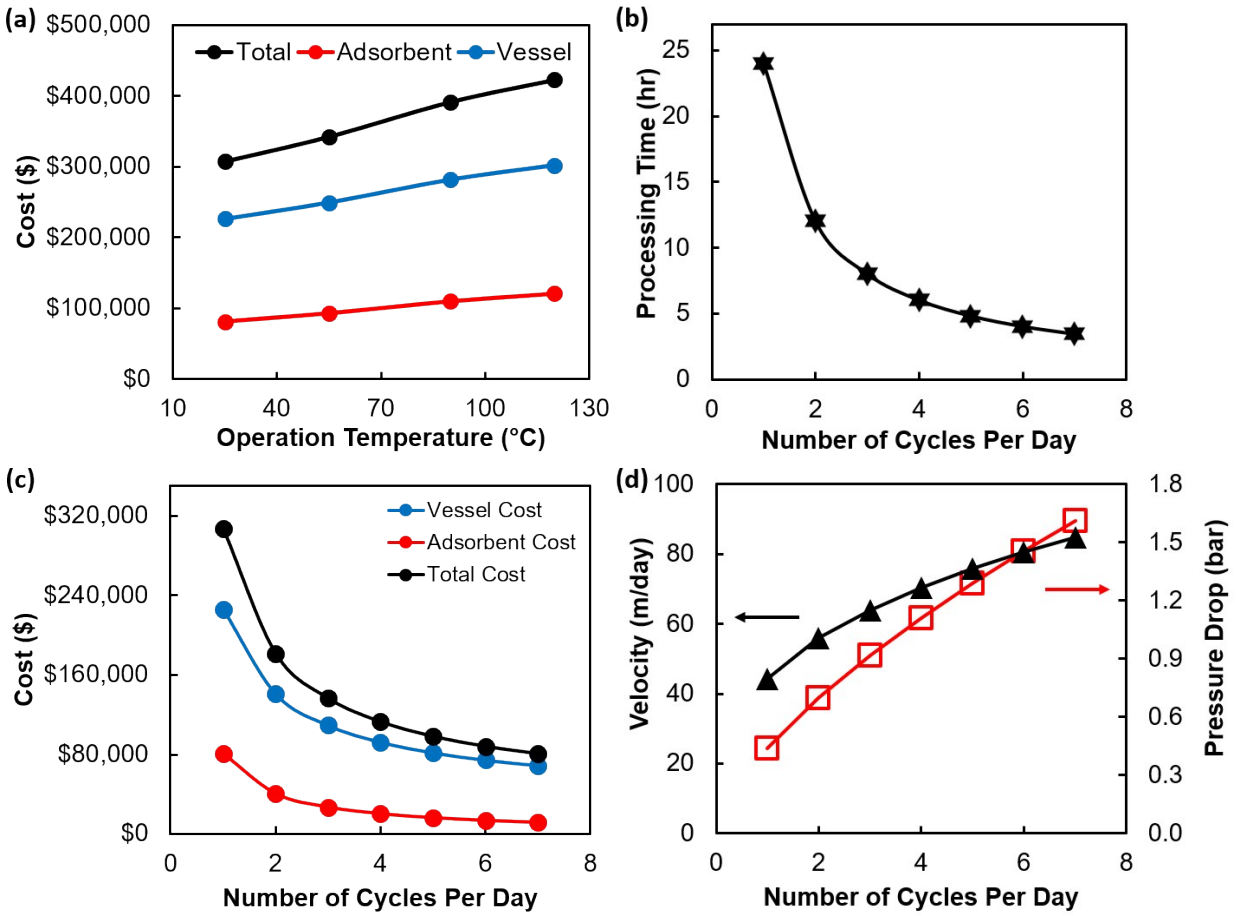

Figure S15: Fixed bed scale-up and cost analysis.

Energy Analysis

The condenser and reboiler heat duties were extracted from Aspen Plus V11. Energy for cooling 300 ton of water/HMF mixture from 103 to 25 °C and heating 270 ton of IPA from 25 to 90 °C per day were calculated using the respective liquid heat capacity. High/Medium/Low pressure steams and 20 °C cooling water were used for utilities. The results are summarized in Table S5.

Table S9: Energy expenditure comparison between distillation columns and the fixed bed adsorption column.

Annual Operational Time [hr]	8000		
Separation Method	**Distillation Column**	**Vacuum Distillation Column**	**Fixed Bed Adsorption**
Condenser Heat Duty [kJ/hr]	-3.02E+07	-3.22E+07	-3.70E+06
Condenser Utility Cost [$/year]	$51,205	$54,689	$6,275
Reboiler Heat Duty [kJ/hr]	3.03E+07	2.96E+07	1.80E+06
Reboiler Utility Cost (HP/MP/ or LP Steam) [$/year]	$629,889 (HP)	$520,103 (MP)	$27,360 (LP)
Total Utility Cost [$/year]	$681,093	$574,792	$33,635

References:

1 T. D. Swift, C. Bagia, V. Nikolakis, D. G. Vlachos, G. Peklaris, P. Dornath and W. Fan, *AIChE J.*, 2013, **59**, 3378–3390.

2 P. Dornath and W. Fan, *Microporous Mesoporous Mater.*, 2014, **191**, 10–17.

3 N. Rajabbeigi, R. Ranjan and M. Tsapatsis, *Microporous Mesoporous Mater.*, 2012, **158**, 253–256.

4 K. Schute, Y. Louven, C. Detoni and M. Rose, *Chemie Ing. Tech.*, 2016, **88**, 355–362.

5 Y. B. Zhang, Q. X. Luo, M. H. Lu, D. Luo, Z. W. Liu and Z. T. Liu, *Chem. Eng. J.*, 2019, **358**, 467–479.

6 C. Detoni, C. H. Gierlich, M. Rose and R. Palkovits, *ACS Sustain. Chem. Eng.*, 2014, **2**, 2407–2415.

7 M. Yabushita, P. Li, H. Kobayashi, A. Fukuoka, O. K. Farha and A. Katz, *Chem. Commun.*, 2016, **52**, 11791–11794.

8 H. Jin, Y. Li, X. Liu, Y. Ban, Y. Peng, W. Jiao and W. Yang, *Chem. Eng. Sci.*, 2015, **124**, 170–178.

9 M. León, T. D. Swift, V. Nikolakis and D. G. Vlachos, *Langmuir*, 2013, **29**, 6597–6605.

10 D. Y. Choi and K. H. Row, *Biotechnol. Bioprocess Eng.*, 2004, **9**, 495–499.

11 V. Specchia and G. Baldi, *Chem. Eng. Sci.*, 1977, **32**, 515–523.

12 A. J. Colombo, G. Baldi and S. Sicardi, *Chem. Eng. Sci.*, 1976, **31**, 1101–1108.

13 V. J. Inglezakis and S. G. Poulopoulos, *Adsorption, Ion Exchange and Catalysis*, Elsevier, 2006.

14 G. Towler and R. Sinnott, in *Chemical Engineering Design: Principles, Practice and Economics of Plant and Process Design*, Butterworth-Heinemann, Elsevier Ltd., Waltham, MA, 2nd edn., 2013.